# A NUMERICAL STUDY OF COMPRESSIBILITY EFFECTS IN TURBULENT MIXING LAYER

**Dongru Li** dli21@uic.edu
**Zia Ghiasi** sghias2@uic.edu
**Jonathan Komperda** jonk@uic.edu
**Farzad Mashayek** mashayek@uic.edu

Department of Mechanical and Industrial Engineering
University of Illinois at Chicago
842 W. Taylor Street, Chicago, Illinois 60607, United States

## ABSTRACT

A direct numerical simulation (DNS) study is carried out to investigate the effects of compressibility in a planar turbulent mixing layer. A high-order discontinuous spectral element method is used for simulating such a compressible flow. The region of laminar-turbulent transition is identified using the frequency spectra and the vorticity characteristics. The compressibility effects in the fully developed turbulent mixing layer are examined by analyzing the autocorrelation functions, the integral time scales, the frequency spectra, and the growth rates of the momentum thickness along the flow direction with different convective Mach numbers. The results show that with increasing the convective Mach number, the autocorrelation decorrelates faster, the integral time scale shortens, the peak of the spectrum is reduced, and the mixing layer growth rate decreases.

## INTRODUCTION

To understand the physics of many important flows, the research on compressible turbulent mixing layer is essential. The simplest way for understanding a turbulent mixing layer is to study the planar mixing layer, which is formed between two parallel fluid streams with different velocities. The effects of compressibility on turbulent mixing layers are investigated in terms of the convective Mach number, which is defined (Bogdanoff, 1983) as

$$M_c = \frac{U_1 - U_2}{c_1 + c_2} \,. \tag{1}$$

Here, $U_1$ and $U_2$ denote the velocities of the fluid in the high- and low-speed streams, respectively; $c_1$ and $c_2$ denote the speeds of sound in the high- and low-speed streams of the mixing layer, respectively. According to the literature, numerical studies on spatially developing turbulent mixing layer are not abundant, very few of which focused on the compressibility effects on the onsets of roll-up and pairing, the spanwise vortices, and the shear layer growth rate. None of the previous studies investigated the effects of compressibility on the position of laminar-turbulence transition and the single-point correlations.

In this work, a direct numerical simulation (DNS) study is conducted to examine the compressibility effects on the turbulent mixing layer. The compressible flow is simulated by a discontinuous spectral element method (DSEM) (Kopriva & Kolias, 1996; Kopriva, 1998; Jacobs *et al.*, 2005). This method has been used for the simulations of the compressible flows in complex geometries (Li *et al.*, 2016; Ghiasi *et al.*, 2016). The main objectives of this work are: (1) to determine the region of laminar-turbulent transition; (2) to identify the mechanism responsible for such transition; (3) to investigate the effects of compressibility on the single-point correlations, the integral time scales, the frequency spectra, and the momentum thickness.

## METHODOLOGY

The full Navier-Stokes equations are employed as the governing equations for the compressible turbulent mixing layer. The vector form of the non-dimensional governing equations can be expressed as

$$\frac{\partial \vec{Q}}{\partial t} + \frac{\partial \vec{F}_i^a}{\partial x_j} - \frac{\partial \vec{F}_i^v}{\partial x_j} = 0 \,, \tag{2}$$

where $\vec{Q}$ is the solution vector; $\vec{F}_i^a$ and $\vec{F}_i^v$ are the advective flux and viscous flux vectors, respectively (for more detail, see Jacobs, 2003). The DSEM is employed to solve the governing equations in a conservative form. The physical domain is partitioned into non-overlapping elements. By using isoparametric mapping, each element is mapped onto a unit hexahedron over the interval $[0,1]$. Consequently, Eq. (2) turns into

$$\frac{\partial \widetilde{Q}}{\partial t} + \frac{\partial \widetilde{F}_i^a}{\partial X_j} - \frac{\partial \widetilde{F}_i^v}{\partial X_j} = 0 \tag{3}$$

where

$$\widetilde{Q} = J\vec{Q} \,,\ \widetilde{F}_i^a = \frac{\partial X_i}{\partial x_j}\vec{F}_j^a \,,\ \widetilde{F}_i^v = \frac{\partial X_i}{\partial x_j}\vec{F}_j^v \,. \tag{4}$$

In Eqs. (2)-(4), the solution vector $\vec{Q}$ and flux vectors $\vec{F}$ are on the physical grid, while $\widetilde{Q}$ and $\widetilde{F}$ are on the mapped grid. $J$ represents the the determinant of the Jacobian matrix, which transforms the elements from the physical space to the mapped space. The term $\partial X_i/\partial x_j$ denotes the transformation matrix, while $x_j$ and $X_i$ indicate the coordinates of the physical space and the mapped space, respectively.

In each element, the solution vector $\widetilde{Q}$ and the flux vectors $\widetilde{F}_i$ in Eq. (3) are calculated by a basis function on the Gauss collocation points and Lobatto collocation points, defined as

$$X_{j+1/2} = \frac{1}{2}\left\{1-\cos\left[\frac{(2j+1)\pi}{2(p+1)}\right]\right\}, \quad j=0,\cdots,p\,, \quad (5)$$

and

$$X_j = \frac{1}{2}\left\{1-\cos\left[\frac{\pi j}{p+1}\right]\right\}, \quad j=0,\cdots,p+1\,, \quad (6)$$

respectively. Here, $p$ represents the polynomial order of the spectral element. The solution vector is approximated as

$$\widetilde{Q}(X,Y,Z) = \sum_{i=0}^{N-1}\sum_{j=0}^{N-1}\sum_{k=0}^{N-1}\widetilde{Q}_{i+1/2,j+1/2,k+1/2}h_{i+1/2}(X)\,h_{j+1/2}(Y)h_{k+1/2}(Z)\,, \quad (7)$$

and similarly for advective and viscous flux vectors (see Jacobs, 2003). Here, X, Y, and Z denote the streamwise, cross-stream, and spanwise coordinates of the mapped space, while $h_{i+1/2}$, $h_{j+1/2}$, and $h_{k+1/2}$ are the Lagrange interpolating polynomials on the Gauss grid. After the solution, advective flux, and viscous flux vectors are computed, a fourth order Runge-Kutta method is adopted for time integration.

## PROBLEM SETUP

The computational grid used in this work for the three-dimensional (3D) compressible turbulent mixing layer simulations is shown in Fig. 1. The size of the computational domain is listed in Table 1 with all dimensions normalized by the initial shear layer momentum thickness, $\delta_\theta(0)$. The momentum thickness, $\delta_\theta$, in a spatial compressible mixing layer, is defined (Jiménez, 2004) as

$$\delta_\theta = \frac{1}{\rho_o}\int_{-\infty}^{+\infty}\langle\rho\rangle\frac{\{u\}-U_2}{\triangle U}\left(1-\frac{\{u\}-U_2}{\triangle U}\right)\mathrm{d}y\,. \quad (8)$$

Here, $\triangle U = U_1 - U_2$; $\rho_o$ denotes the initial inflow density; $\langle\rho\rangle$ and $\{u\}$ denote the Reynolds-averaged density and the Favre-averaged velocity, respectively.

The region used to study the flow properties for all cases is $0 \le x \le 1200$. The rest of the domain is employed as a buffer zone to avoid solution contamination from the outlet boundary. The computational domain is discretized contingent on the flow configuration. Such non-uniform grid distribution is employed to ensure a finer grid in the mixing layer as shown in Fig. 1, which is a two-dimensional (2D) baseline grid on the $x-y$ plane. This 2D baseline grid is then extruded uniformly in the spanwise direction to construct a 3D mesh, which consists of 68,442 elements. In this study, two polynomial orders, $p$ = 5 and 7, are employed, resulting in a total of 14,783,472 and 35,042,304 solution points, respectively.

Table 1. $L_x$, $L_y$, and $L_z$ are the computational domain dimensions normalized by $\delta_\theta(0)$, while $N_x$, $N_y$, and $N_z$ indicate the corresponding numbers of solution points for $p = 5$.

| $L_x \times L_y \times L_z$ | $N_x \times N_y \times N_z$ |
|---|---|
| $1782 \times 800 \times 283$ | $1098 \times 204 \times 66$ |

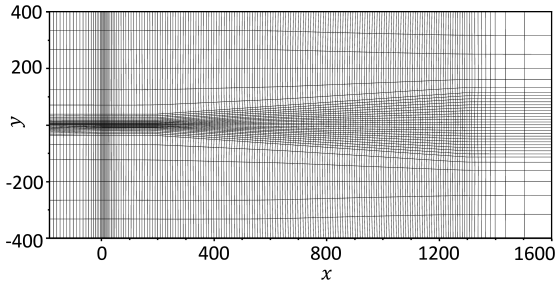


Figure 1. Computational grid showing only elements.

The computational domain is bounded by the inflow and outflow boundaries in the streamwise direction, the non-reflecting boundaries in the cross-stream direction, and the periodic boundaries in the spanwise direction. The schematic of such setup is illustrated in Fig. 2. The boundary layer inlet condition investigated by McMullan *et al.* (2009) is used as inflow condition in this work. The free-stream velocities in the high- and low-speed sides are set to satisfy the velocity ratio, $R = 0.54$, for all simulations, where $R = (U_1 - U_2)/(U_1 + U_2)$. The Reynolds number, $Re_\theta$, based on $\triangle U$ and $\delta_\theta(0)$, is selected as 175, with the consideration that it is small enough for resolving the flow but large enough for the transition to turbulence. A small turbulence intensity (less than 0.5% of the maximum streamwise inlet velocity), generated by a stochastic model (Gao & Mashayek, 2004), is superimposed on the inlet condition. Density and temperature are uniformly initialized to 1.0 and $(\triangle U\,/\,2M_c)^2$, respectively. To damp any nonphysical high wavenumber oscillations at the outlet boundary, a

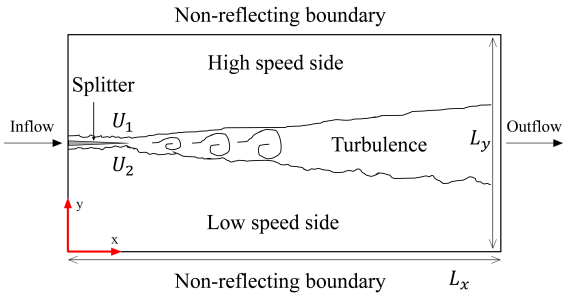


Figure 2. The schematic of the computational domain.

buffer zone near the boundary is employed and a damping-sponge is accomplished by grid stretching.

## VALIDATION AND CONVERGENCE STUDY

Three simulations are conducted with different inflow Mach numbers and convective Mach numbers, as shown in Table 2. The case Mc1 is selected as a reference case for the baseline incompressible flow comparisons, since $M_c$ = 0.1 is adequately small to consider the effects of compressibility negligible. The spectral multidomain method allows the spatial resolution to be adjusted in two ways: changing the number of elements (h-refinement) and modifying the polynomial order within an element (p-refinement). The h-refinement gives an algebraic convergence rate, whereas an exponential convergence rate is provided by p-refinement (Karniadakis & Sherwin, 1999). Thus, a p-convergence study is carried out for the baseline cases with two different polynomial orders, $p = 5$ and 7. Our baseline DNS results are then compared with computational and experimental results for incompressible mixing layer.

Table 2. Inflow Mach numbers in the high- and low-speed sides are defined as $M_1 = U_1/c_1$ and $M_2 = U_2/c_2$, respectively.

| Case | $M_1$ | $M_2$ | $M_c$ |
|---|---|---|---|
| Mc1 | 0.2857 | 0.0857 | 0.1 |
| Mc2 | 0.5704 | 0.1704 | 0.2 |
| Mc3 | 0.8555 | 0.2556 | 0.3 |

To perform the comparison for the degree of self-similarity, two profiles of the Favre-averaged streamwise velocity, $\{u\}$, are extracted from two cross-stream lines (y-line) at $x = 667$ and 1167, both located in the self-similar turbulent region (See Fig. 6). The comparison with the experimental profile obtained by D'Ovidio (1998) is presented in Fig. 3. In this figure, $x_0$ and $y_{0.5}$ are the origin of the mixing layer and the lateral position at which the streamwise velocity approaches the value of convective velocity in the cross-stream direction, respectively. The convective velocity, $U_c$, is defined as $U_c = (c_2U_1 + c_1U_2)/(c_1 + c_2)$. Figure 3 shows the following: an excellent self-similarity is achieved; a good agreement between the results from $p = 5$ and 7 is observed; the discrepancy between the results from the present DNS and the previous experiment is small.

Figure 4 shows the similarity profiles of the streamwise Reynolds stress compared against the results obtained by other researchers. The peak of the normal stress is 0.0322 in the case with $p = 5$, 0.0320 with $p = 7$, 0.0310 in the experimental data obtained by D'Ovidio (1998), and 0.0283 in the LES conducted by McMullan *et al.* (2009). The peaks of the normal stress and the self-similar shapes are in good agreement with both previous results. However, compared to the result of McMullan *et al.* (2009), both results obtained by the current study for $p = 5$ and 7 have better agreements with the experimental result. Based on the above comparisons, it is concluded that the resolutions obtained with two polynomial orders, $p = 5$ and 7, are both acceptable. Therefore, the polynomial order used for further simulations is taken as $p = 5$ with the consideration of the computational cost.

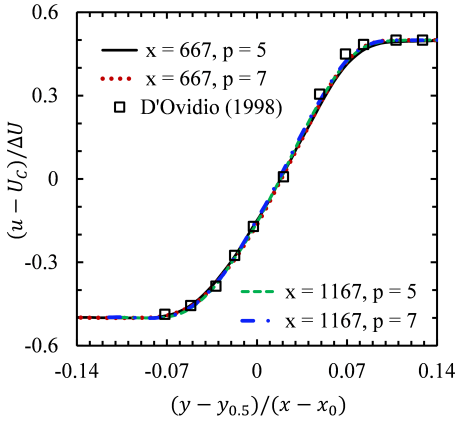


Figure 3. Comparison of the profiles of the streamwise mean velocity for different polynomial orders at two locations to the experimental results of D'Ovidio (1998).

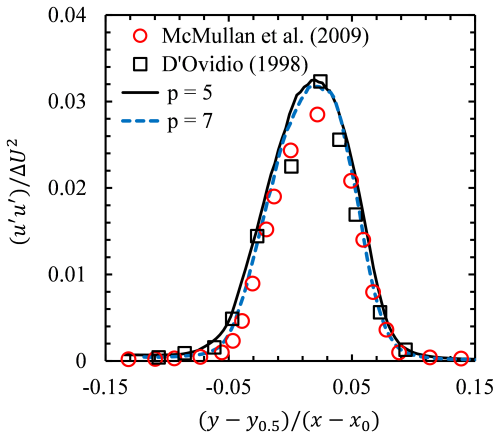


Figure 4. Comparison of the similarity profiles of streamwise Reynolds stresses with LES of McMullan *et al.* (2009) and experiment of D'Ovidio (1998).

## LAMINAR-TURBULENT TRANSITION ZONE

To ensure the data used for analyzing the effects of compressibility on the turbulent shear layer is extracted from the self-similar turbulent region, the location of the laminar-turbulent transition zone is needed to be identified. In this work, the transition region is estimated by analyzing the behavior of the frequency spectrum and the characteristic of the instantaneous flow.

In a self-similar turbulent region, the velocity frequency spectra display the power-law behavior with the exponent of $-5/3$ in the inertial subrange (Pope, 2000). The streamwise velocity frequency spectrum is defined as

$$E_u(f) = \int_{-\infty}^{\infty} R_u(s)\, e^{-i2\pi fs} ds\,, \tag{9}$$

where

$$R_u(s) = \langle u'(t)u'(t+s)\rangle\,. \tag{10}$$

Here, $f$ is the frequency; $s$ and $u'$ are the time lag and the fluctuation of streamwise velocity, respectively. $R_u(s)$ denotes the streamwise velocity autocovariance. In its normalized form, the autocorrelation function of the streamwise velocity is

$$\Upsilon_u(s) = \frac{R_u(s)}{\langle u'^2(t)\rangle}, \tag{11}$$

similarly for $\Upsilon_v$ and $\Upsilon_w$, which are the autocorrelation functions of cross-stream and spanwise velocity components.

Figure 5 shows the frequency spectra of the streamwise velocity at four locations listed in Table 3. At probe A, the behavior of the frequency spectrum reflects the fundamental Kelvin-Helmholtz instability, and therefore the flow is not turbulent in this region. As the flow proceeds downstream to probes B, C, and D, the exponent of the spectrum in the roll-off converges towards the exponent of -5/3, indicating that the flow is in transition to turbulence.

Table 3. Locations of four probes along the centerline of the mixing layer.

| Probe | A | B | C | D |
|---|---|---|---|---|
| x | 113 | 339 | 565 | 791 |

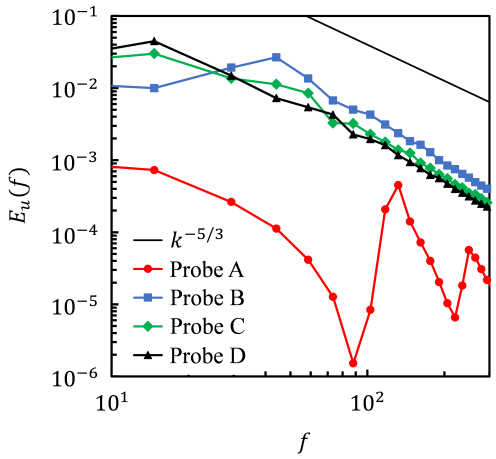


Figure 5. Frequency spectra of streamwise velocity at different locations.

The contours of the spanwise vorticity with convective Mach number of $M_c = 0.1$ are shown in Fig. 6. It is seen that the large coherent vortices emerge at $x \approx 100$, then interact mutually toward downstream, and eventually breakdown to small-scale structures at approximately $300 \leq x \leq 600$. The region $100 < x < 600$ is indicated by white dashed line, which approximates the zone of the laminar-turbulent transition.

Ho & Huang (1982) proposed that the formation of secondary streamwise vortices and the breakdown of primary spanwise vortices are responsible for the onset of turbulence transition. In this context, we consider a 3D representation of turbulent structures via an iso-surface and volume rendering technique, which is shown in Fig. 7. The 2D primary spanwise coherent structures can be seen in $100 < x < 300$ in the mixing layer. In the braid region, the 3D secondary streamwise vortex structures emerge along with the primary coherent structures. These secondary streamwise vortices then stretch the primary spanwise vortices to breakdown into small-scale structures, roughly in the region $300 < x < 600$. These observations are consistent with the study by Pierrehumbert & Widnall (1982), suggesting that the mutual interaction between 2D and 3D instabilities significantly facilitates the transition from laminar to turbulence in mixing layers and thus leads to a self-similar turbulent state. This process is the primary mechanism accounting for both the formation of the vortex structures and the transition to turbulence. Hence, the entire turbulence transition is roughly in the region of $100 < x < 600$.

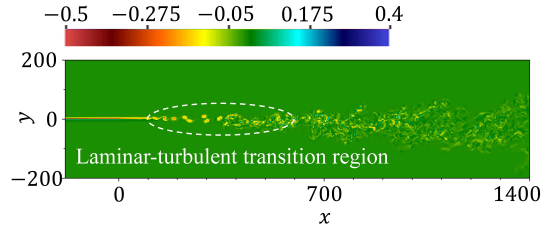


Figure 6. Contours of the spanwise vorticity in the case with $M_c = 0.1$.

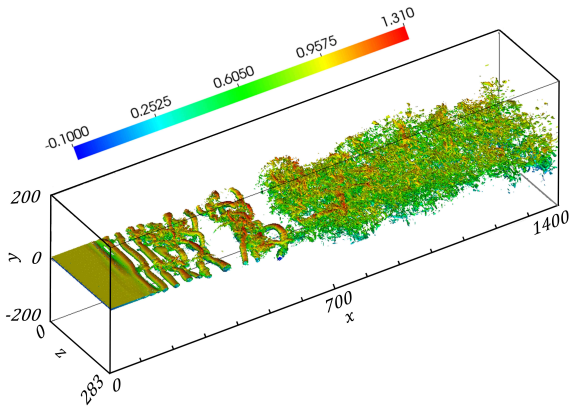


Figure 7. Iso-surface of vorticity magnitude colored by the streamwise velocity.

## COMPRESSIBILITY EFFECT IN TURBULENT MIXING LAYER

The effects of convective Mach number are studied through the analysis of the autocorrelation functions, the integral time scales, the frequency spectra, and the growth rates of the momentum thickness along the streamwise direction with different convective Mach numbers.

### Autocorrelation Functions and Integral Time Scales

Figure 8 shows the autocorrelation functions of the streamwise, cross-stream, and spanwise velocities at $x =$

719 on the centerline of the mixing layer for various convective Mach numbers. For the same convective Mach number, the autocorrelation functions of all three velocity components display a similar trend. The case with high convective Mach number, $M_c = 0.3$, shows a steeper roll-off in the autocorrelation function (faster decay to zero) than does the case with the low convective Mach number, $M_c = 0.1$. A steep roll-off of the autocorrelation function denotes the high-frequency velocity fluctuations, which are directly related to the smallest-scale vortex structures, and vice versa.

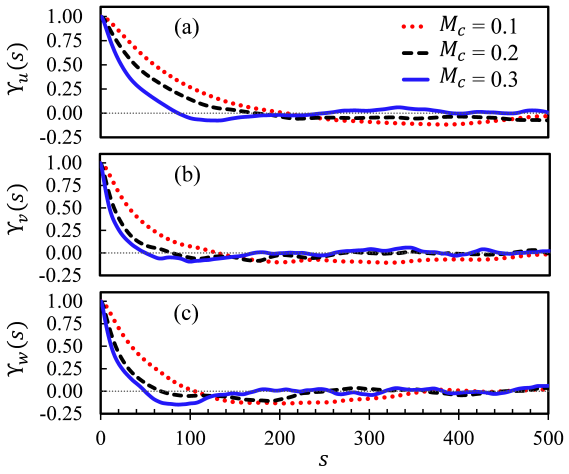


Figure 8. Autocorrelation functions of (a) streamwise velocity, (b) cross-stream velocity, and (c) spanwise velocity, for various convective Mach numbers.

The longest connection in the turbulent behavior over time can be measured via the integral time scale, defined as

$$\tau_u = \int_0^\infty \Upsilon_u(s)\, ds\,, \tag{12}$$

and similarly for $\tau_v$ and $\tau_w$. Here, $\tau_u$, $\tau_v$, and $\tau_w$ denote the integral time scales of $u$, $v$ and $w$ velocity fluctuations, respectively. The integral time scales for the cases with different convective Mach numbers are presented in Fig. 9. This figure indicates that with increasing the convective Mach number, the integral time scale decreases. Therefore, it can be deduced that at any stationary planar turbulent mixing layer, an increase in the convective Mach number may lead to a reduction in the sizes of largest-scale structures. Also, Fig. 9 shows that the magnitudes of $\tau_v$ and $\tau_w$ are nearly identical, and that both the ratios of $\tau_u/\tau_v$ and $\tau_u/\tau_w$ are approximately equal to 2.

## Frequency Spectra

The frequency spectra of the streamwise velocity at $x = 719$ on the centerline of the mixing layer for different convective Mach numbers are shown in Fig. 10. It can be seen that in the roll-off of the spectra, all of them show the power-law behavior with the exponent of $-5/3$. However, this power-law behavior appears sooner (at the lower frequency range) for the low convective Mach number case, $M_c = 0.1$, than that for the high convective Mach number case, $M_c = 0.3$. Also, as the convective Mach number increases, the peak of the spectrum decreases. This finding

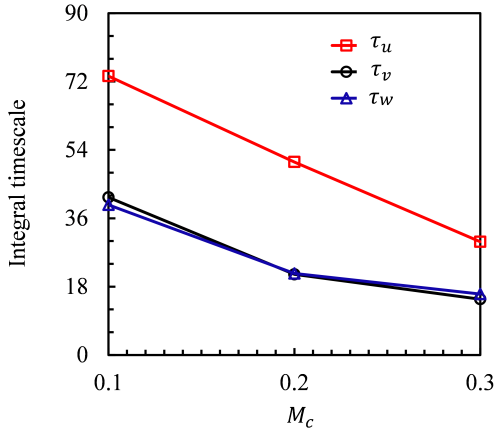


Figure 9. Integral times-cales for different convective Mach numbers.

is consistent with those results shown in Fig. 9. Observations from both Figs. 9 and 10 indicate that an increase in $M_c$ leads to a decrease in the sizes of the largest-scale structures.

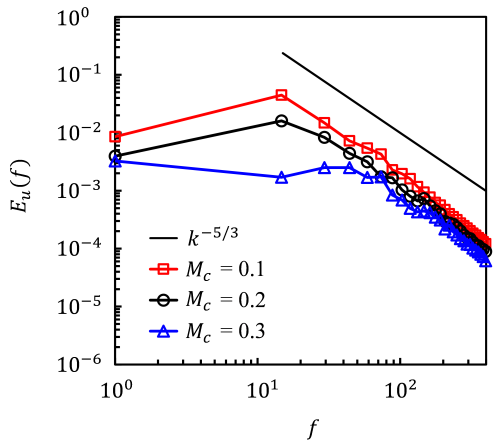


Figure 10. Frequency spectra of the streamwise velocity for different convective Mach numbers.

## Growth of Momentum Thickness

Figure 11 presents the evolution of the momentum thickness $\delta_\theta(x)$ along the streamwise direction for different convective Mach numbers. For better comparison, linear trendlines are also included for the self-similar turbulent region for three cases. The growth rates of the momentum thickness in the self-similar turbulent region are computed as 0.0239, 0.0198, and 0.0173 for the corresponding convective Mach numbers of 0.1, 0.2, and 0.3, respectively. It is concluded that as the convective Mach number increases, the growth rate of the momentum thickness decreases. This observation is consistent with the experimental results from Papamoschou & Roshko (1988) and Goebel & Dutton (1991). It has also been suggested that the slow growth of the mixing layer occurs at higher convective Mach numbers mainly due to the reduced growth rate of linear instability (Lele, 1989).

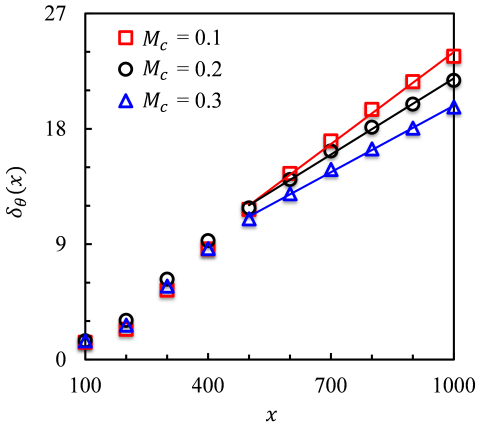


Figure 11. Evolution of the momentum thickness for different convective Mach numbers.

## CONCLUSIONS AND FUTURE WORK

Direct numerical simulations have been conducted for spatially developing plane turbulent mixing layer, employing a high-order discontinuous spectral element method. The laminar-turbulent transition occurs within the computational domain, and the region of the transition is approximated by analyzing the behaviors of frequency spectra and the scales of the vortex structures. The mechanism responsible for the production of small-scale vortex structures is the spanwise stretching driven by the secondary streamwise vortices. Compressibility effects on the fully developed turbulent mixing layer are investigated via the autocorrelation functions, the integral time scales, the frequency spectra, and the momentum thickness growth rates. As the convective Mach number increases, the autocorrelation decorrelates faster, the integral time scale shortens, the maximum of the spectrum is reduced, and the mixing layer growth rate decreases.

For future work, we plan to further investigate the effect of compressibility on the location and length of the turbulent transition zone by analyzing the flow properties in the transition region, such as normal Reynolds stress and the budget terms of turbulent kinetic energy.

## ACKNOWLEDGMENTS

The computational resources for this study were provided by UIC Extreme (High Performance Computing Cluster) at the University of Illinois at Chicago. The Program Development Company GridPro provided the authors with troubleshooting support and license to access its meshing software, which was used to create the meshes for the simulations presented in this study.

## REFERENCES

Bogdanoff, D. W. 1983 Compressibility effects in turbulent shear layers. *AIAA J.* **21**, 926–927.

D'Ovidio, A. 1998 Coherent structures in turbulent mixing layers. Ph.D. Thesis, University of Leicester, Leicester, UK.

Gao, Z. & Mashayek, F. 2004 Stochastic model for non-isothermal droplet-laden turbulent flows. *AIAA J.* **42**, 255–260.

Ghiasi, Z., Komperda, J., Li, D. & Mashayek, F. 2016 Simulation of supersonic turbulent non-reactive flow in ramp-cavity combustor using a discontinuous spectral element method. AIAA Paper 2016-0617.

Goebel, S. G. & Dutton, J. C. 1991 Experimental study of compressible turbulent mixing layers. *AIAA J.* **29**, 538–546.

Ho, C-M. & Huang, L-S. 1982 Subharmonics and vortex merging in mixing layers. *J. Fluid Mech.* **119**, 443–473.

Jacobs, G. B. 2003 Numerical simulation of two-phase turbulent compressible flows with a multidomain spectral method. Ph.D. Thesis, University of Illinois at Chicago, Chicago, IL.

Jacobs, G. B., Kopriva, D. A. & Mashayek, F. 2005 Validation study of a multidomain spectral code for simulation of turbulent flows. *AIAA J.* **43**, 1256–1264.

Jiménez, J. 2004 Turbulence and vortex dynamics. *Notes for the Polytechnic Course on Turbulence* .

Karniadakis, G. E. & Sherwin, S. J. 1999 *Spectral/hp element methods for CFD*. New York, NY: Oxford University Press.

Kopriva, D. A. 1998 A staggered-grid multidomain spectral method for the compressible Navier-Stokes equations. *J. Comput. Phys.* **143**, 125–158.

Kopriva, D. A. & Kolias, J. H. 1996 A conservative staggerd-grid Chebyshev multidomain method for compressible flows. *J. Comput. Phys.* **125**, 244–261.

Lele, S. K. 1989 Direct numerical simulation of compressible free shear flows. AIAA Paper 1989-0374.

Li, D., Ghiasi, Z., Komperda, J. & Mashayek, F. 2016 The effect of inflow mach number on the reattachment in subsonic flow over a backward-facing step. AIAA Paper 2016-2077.

McMullan, W. A., Gao, S. & Coats, C. M. 2009 The effect of inflow conditions on the transition to turbulence in large eddy simulations of spatially developing mixing layers. *Int. J. Heat Fluid Flow* **30**, 1054–1066.

Papamoschou, D. & Roshko, A. 1988 The compressible turbulent shear layer: An experimental study. *J. Fluid Mech.* **197**, 453–477.

Pierrehumbert, R. T. & Widnall, S. E. 1982 The two and three dimensional instabilities of a spatially periodic shear layer. *J. Fluid Mech.* **114**, 59–82.

Pope, S. B. 2000 *Turbulent flows*. Cambridge, UK: Cambridge University Press.